Vol. 267: 27–43, 2004 | MARINE ECOLOGY PROGRESS SERIES
Mar Ecol Prog Ser | Published February 19

Contribution of fine-scale vertical structure and swimming behavior to formation of plankton layers on Georges Bank

Scott M. Gallager[1,*], Hidekatsu Yamazaki[1,2], Cabell S. Davis[1]

[1]Woods Hole Oceanographic Institution, Woods Hole, Massachusetts 02543, USA
[2]Department of Ocean Sciences, Tokyo University of Fisheries, 4-5-7 Konan, Minato-ku, Tokyo 108-8477, Japan

ABSTRACT: The roles of plankton behavior, stratification, and microstructure in the formation of fine-scale plankton layers were examined using a 3-dimensional video plankton recorder mounted on a remotely operated vehicle. Vertically compressed plankton patches were observed in association with a cold pool over the Southern Flank of Georges Bank, extending from the tidal mixing front to the shelf-slope break during the months of May and June, 1994, 1995, 1997. In June 1995, 3 major plankton layers were present: a 10 m thick layer above the thermocline, a 1 m thick layer within the thermocline, and a third, 2 to 5 m thick layer immediately below the thermocline. Energy dissipation rate was lowest in the central layer and increased in both top and bottom layers. Some passive organisms and particles, e.g. the colonial diatom *Chaetoceros socialis* and rod-shaped diatoms, were concentrated in all 3 layers, while marine snow particles were found only in transitional regions. All stages of *Calanus* spp. were present in high numbers on the fringes of all 3 layers, while *Oithona* sp. was found only in the thin, central layer. Plankton were significantly aggregated only when the motility number, Mn (i.e. ratio of plankton swimming speed/rms turbulent velocity) was greater than 3, suggesting dominance of plankton behavior over physical structure. Under both quiescent and turbulent conditions, the Lagrangian frequency spectra (f) for swimming plankton and passive particles decreased with a slope of f^{-2}. However, in quiescent conditions, the magnitude of the spectrum for swimming plankton was 10-fold greater than for passive particles, illustrating a decoupling of plankton swimming from turbulent eddies. The air/water interface, the pycnocline, and multiple shear interfaces at density discontinuities act as boundaries to vertical zones where plankton behavior may succumb to or dominate background microstructure, thus providing a mechanism for formation of plankton and particulate layers.

KEY WORDS: Fine-scale vertical structure · Thin layers · Plankton behavior · Turbulence

INTRODUCTION

Although it is generally recognized that coupling between physical and biological processes modulates abundance and species composition of plankton in the world oceans, the dominant scales of these interactions are poorly understood (Denman & Powell 1984, Mackas et al. 1985, Yamazaki et al. 2002). Meso-scale spatial heterogeneity in zooplankton distributions has been observed for over a century, and was formally quantified more than 50 yr ago (Hardy & Gunther 1935). While numerous subsequent studies related plankton spatial structure to hydrographic and physical structure, fine-scale (i.e. m) and microscale (i.e. mm to cm) patterns are generally thought to be stochastic and ephemeral in nature (e.g. Fasham 1978). If this is true, estimates of primary and secondary production in the world oceans based on random fluctuations in small-scale plankton distributions would average out, thus requiring only very coarse sampling of the plankton community to describe its composition. However, more recent studies have shown that within plankton

*Email: sgallager@whoi.edu

communities, species-specific patterns in abundance can form as a function of fine-scale physical structure (Owen 1989, Davis et al. 1992, Gallager et al. 1996b) and may persist for many days (Donaghay et al. 1992, Cowles & Desiderio 1993, reviewed in Cowles et al. 1998). If this scale is undersampled or, worse, ignored, the result of persistent fine-scale structure will be gross underestimates of production (Cowles et al. 1998).

Vertical fine-structure has been observed since the study of Eckart (1948), and is usually described in terms of mixing, such as the interaction between density stratification and horizontal shear (Gargett et al. 1984). One of the net results of shear is to redistribute horizontal variance onto vertical variance, producing the typical multiple-layer effect, or steps, commonly observed in CTD profiles of stratified water columns (Eckart 1948, Kullenberg 1978, Osborn 1998). Intrusion of adjacent water masses (Ochoa 1987) and production of ephemeral structures related to the breaking of internal waves (Franks 1995) are also possible mechanisms for fine-structure formation.

Layers of plankton and particles can form in association with vertical fine-structure by both common and unique mechanisms. Both non-motile particles such as marine snow and motile plankton may simply be redistributed by shear along with a water mass as shown in the unique dye experiments of Kullenberg (1978). Particles and plankton may also accumulate at density discontinuities at the base of the mixed layer (Land & Wood 1987) and above the pycnocline (MacIntyre et al. 1995) through a reduction in sinking speed as they enter regions of greater density and viscosity (Gallager et al. 1996a). A mechanism available to motile plankton alone is the ability to swim in an organized and directed manner into a desired region and form aggregations at local concentrations which greatly exceed those that would be expected if a population were randomly distributed.

When would we expect plankton to follow local flow and when should they be able to swim independently of turbulence and form aggregations? The local microscale environment of plankton in which feeding and mate location take place is quite different physically from the fine-scale distances over which vertical migration may occur. Therefore, this question must be addressed as a function of scale, whether it be body size, volume of the flow field generated by the swimming and feeding organism, or a characteristic length scale determined by the swimming pattern. Turbulent energy dissipation at the ocean surface ranges from 10^{-5} to 10^{-4} W kg^{-1}, decreasing with increasing depth to about 10^{-6} W kg^{-1} within 10 m (Yamazaki & Kamykowski 1991, Osborn et al. 1992) and to about 10^{-7} to 10^{-10} W kg^{-1} in the stratified depths of the ocean (Gargett 1989). Yamazaki & Squires (1996) used the Ozmidov scale to relate the turbulence energy spectrum to the root mean square (rms) turbulence velocity. They suggested that many plankton, increasing in size from large protozans to copepods and decapods, are capable of swimming independently of local flow when their swimming speed is equal to or greater than rms turbulence velocities. Although rms velocities vary considerably with depth, wind stress and internal shear, the results of Yamazaki & Squires (1996) provide a direct means of comparing plankton swimming capacity with ambient turbulence. Thus, plankton may be dependent on local flow for their transport, or may possess some ability to swim independently as they migrate through regions of the water column where dissipation rates span >6 orders of magnitude. Their transport will be directly related to the swimming speed of the individual plankton species and local, uncorrelated fluctuations in turbulence velocity. To understand how plankton behavior and swimming potential contribute to the formation of plankton layers in the ocean, physical variables must be measured to calculate density gradient and shear, together with simultaneous measurements of rms turbulence velocities and plankton swimming speeds. Although this has been accomplished in the laboratory in confined vessels (Saiz 1994), *in situ* measurements have not been made.

The present study was part of the US Global Ocean Ecosystems Dynamics (GLOBEC) program on Georges Bank in the NW Atlantic Ocean. Our intention was to observe and quantify vertical distributions and behavior of plankton in relation to the prevailing physical fine-structure and microstructure. Questions we addressed were: (1) What are the potential physical and biological mechanisms of the accumulation of non-motile particulates and aggregation of swimming plankton into discrete vertical layers? (2) What is the relationship between plankton swimming speed and aggregation with reference to background flow? During the cruise, a towed video plankton recorder (VPR) was used to obtain mesoscale structure and plankton distributions for comparison with the results reported in this study; the results of this comparison will appear elsewhere.

MATERIALS AND METHODS

Physical setting. As part of a series of US GLOBEC cruises to Georges Bank during the spring of 1995 on RV 'Endeavor' Cruise EN267, we sampled intensively in the Southern Flank region using the towed VPR and a 3-dimensional imaging system (3DVPR) on the remotely controlled vehicle (ROV) 'Jason'. On June 16, 1995, a linear transect was made with the towed VPR (Transect 15) between 00:37 and 09:17 h; the transect

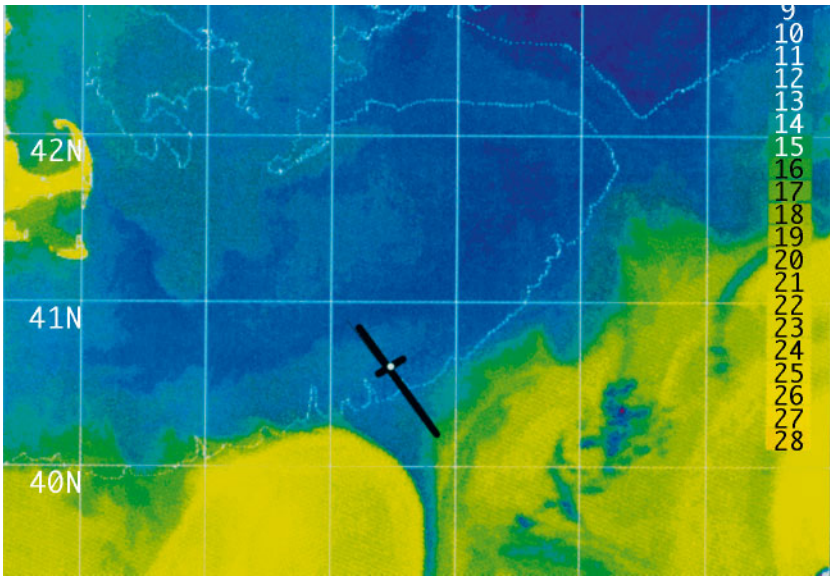

Fig. 1. Advanced very high-resolution radiometry showing sea-surface temperature (°C) in Georges Bank region on June 17, 1995. Note warm-core rings impacting the Southern Flank at about the 200 m isobath. Video plankton recorder (VPR) Transect 15 is shown as black line extending southeast from the 70 to the 200 m isobath, with remotely operated vehicle (ROV) Jason deployment indicated by cross

extended 52 km from the Southern Flank to the shelf edge (Fig. 1). The VPR was undulated from the surface to 10 m off the bottom while data on temperature, salinity, density, fluorescence and light transmission, along with images from the VPR, were plotted and viewed in real-time. The real-time display of the VPR showed the edge of a warm-core ring adjacent to cooler shelf water and a subsurface chlorophyll maximum at about 40 m (Fig. 2). After completing the transect, we doubled-back to deploy the ROV and 3DVPR, returning to a location where the chlorophyll maximum was most intense. The deployment reported here was at 4034.19 N and 6740.51 W, about 18 km west of the beginning of VPR Transect 15.

Density was calculated from salinity and temperature sampled at a frequency of 3 Hz using Sea Bird sensors mounted on the ROV. Data from the ship's RD Instruments (RDI) 150 kHz acoustic doppler current profiler (ADCP) were binned into 3 m bins, and the ship's motion was subtracted using bottom-tracking. Shear was calculated as described in Gallager et al. (1996b) from the difference in velocity between the centers of each bin as:

$$\partial u/\partial z = [(\partial u_i/\partial z)^2 + (\partial u_j/\partial z)^2]^{1/2} \quad (1)$$

where u_i and u_j are the northerly and easterly components of velocity (u) and z is depth. Richardson numbers (Ri) were calculated from Brunt-Vaisala frequencies (N^2) and shear stress, where $N^2 = -g/\rho(\partial\rho/\partial z)$, ρ is density, and $Ri = N^2/(\partial u/\partial z)^2$. Density profiles were filtered to correspond with the 3 m bins used for the calculation of shear. Both density and shear were interpolated to a common depth, using cubic splines before calculation of N^2 and Ri.

The critical Ri used to indicate the likelihood of mixing through turbulent instability depends on the scale over which density and shear have been measured. Ri critical has been experimentally determined as 0.25 when density and shear are measured at scales of centimeters, and closer to 1 when values are averaged over scales of meters (Kundu & Beardsley 1991, Yamazaki & Osborn 1993). Because of sampling constraints with the ADCP, our averages of shear over 3 m bins suggest that a more conservative critical Ri value should be used. For this reason, we consider Ri <1 to indicate regions where shear instabilities result in mixing on scales of meters.

Optical sampling techniques. The ROV 'Jason' was used to position the imaging system at various depths in the water column and collect data on plankton swimming behavior and motion of passive particles in 3D. To compensate for passive torque and thus minimize thruster usage, 'Jason' was trimmed to neutral buoyancy at a depth of 10 m with coincident centers of gravity and buoyancy. Changes in buoyancy with depth were not sufficient to affect vehicle performance. The imaging system consisted of a 2-axis 3DVPR system mounted on a 2 m-square frame affixed to the front of ROV 'Jason' (Fig. 3a). The separation distance between each camera and its paired strobe was 2 m and the distance of the frame to the front of 'Jason' was 2 m. The cameras were aligned on orthogonal axes with concentric image volumes, such that the view of one camera was from the top looking down (X–Y plane, Fig. 3b), and the other was from the side looking laterally into the water column (Y–Z plane, Fig. 3c). Magnification of both cameras was set with appropriate lenses to a field of view (FOV) of 6.1 × 5.2 × 7.3 cm (width × height × depth). The strobe beams were fitted with a long pass-filter (Schott No. RG715) with 50% transmission at 715 nm, collimated to a diameter of ca. 10 cm, and directed across the image volume 8° off camera axis. The resulting forward-scattered and diffracted light produced a high-contrast image with particles appearing bright against a dark background (see images in Gallager et al. 1996b).

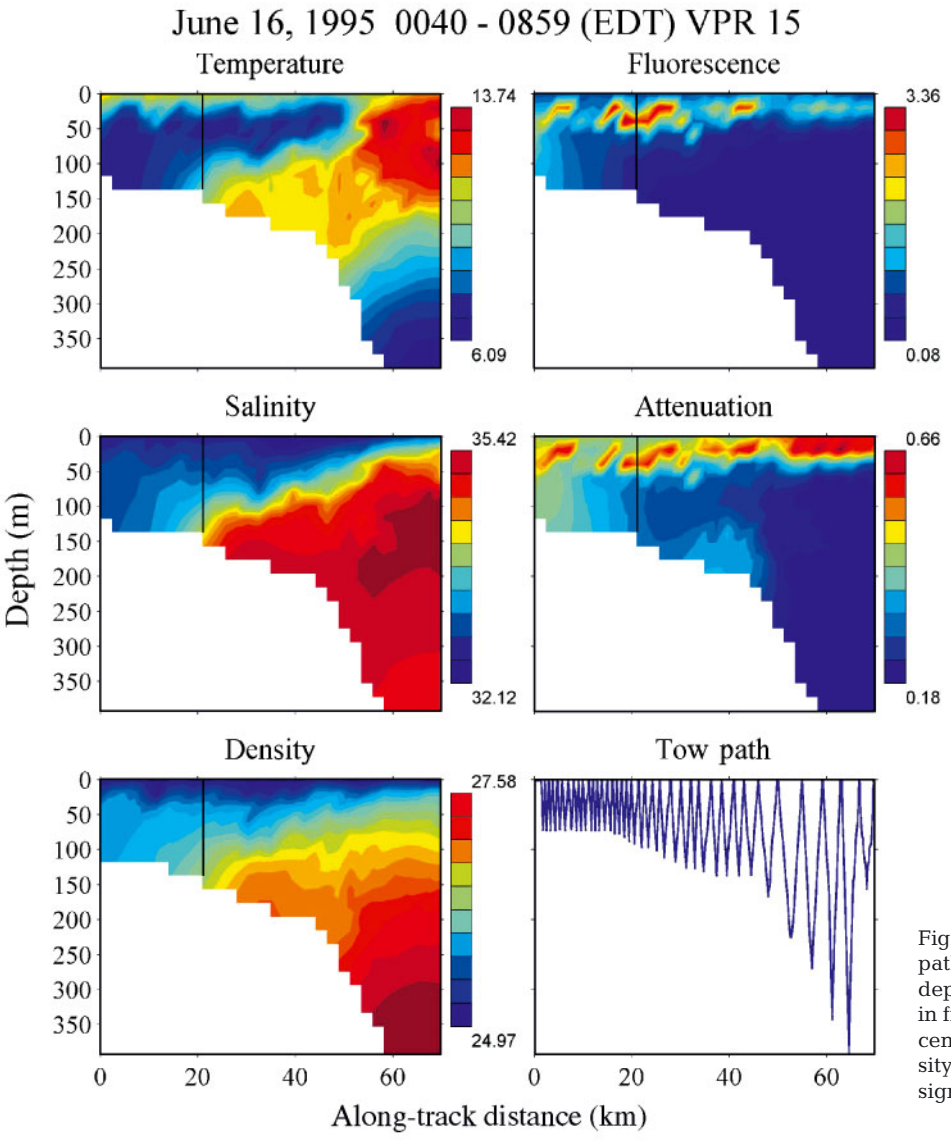

Fig. 2. Hydrographic data and tow path for VPR Transect 15. ROV 'Jason' deployment indicated by vertical line in first 5 graphs. Temperature, fluorescence, salinity, attenuation and density units = °C, volts, psu, units/m, and sigma-t, respectively. EDT: Eastern Daylight Time

Calibration. The concentricity and 3D registration of the 2 orthogonal cameras were established using a $2 \times 2 \times 2$ cm Plexiglas cube held in the FOV. The image volume was defined by transferring the spatial dimensions from the 8 corners of the cube to the X–Y and Y–Z images, which were then combined to form a 3D image (Fig. 3d; see subsection 'Data processing' below). Temporal and spatial resolutions were 0.016 s and ~100 µm, respectively.

Recording. The video signals from both cameras were modulated onto a fiber-optic cable, transmitted to the surface, demodulated, and recorded on separate Betacam SP recorders. Video signals were displayed side by side for piloting purposes. A time-code generator inserted field-accurate (1/60 s) time into the video signals of both cameras during recording, allowing precise time-matching of the video. A 1 kHz tone was inserted into the audio tracks to signal the video-digitizing hardware to begin and end data extraction (see below).

Environmental sensors. A complete suite of environmental sensors was mounted on the ROV, including Sea Bird temperature, conductivity and pressure sensors, a Sea Tek fluorometer configured for chlorophyll, and a transmissometer configured for maximum absorption at 520 nm. Environmental data were recorded at 3 Hz and plotted in real-time at the surface.

Sampling protocol. A total of 7 deployments with ROV 'Jason' were made during Cruise EN267; 3 in the well-mixed area inside the 60 m isobath, 3 in stratified water on the Southern Flank, and 1 outside the shelf-break front along the 200 m isobath. After some experimentation, we found that the most efficient sampling

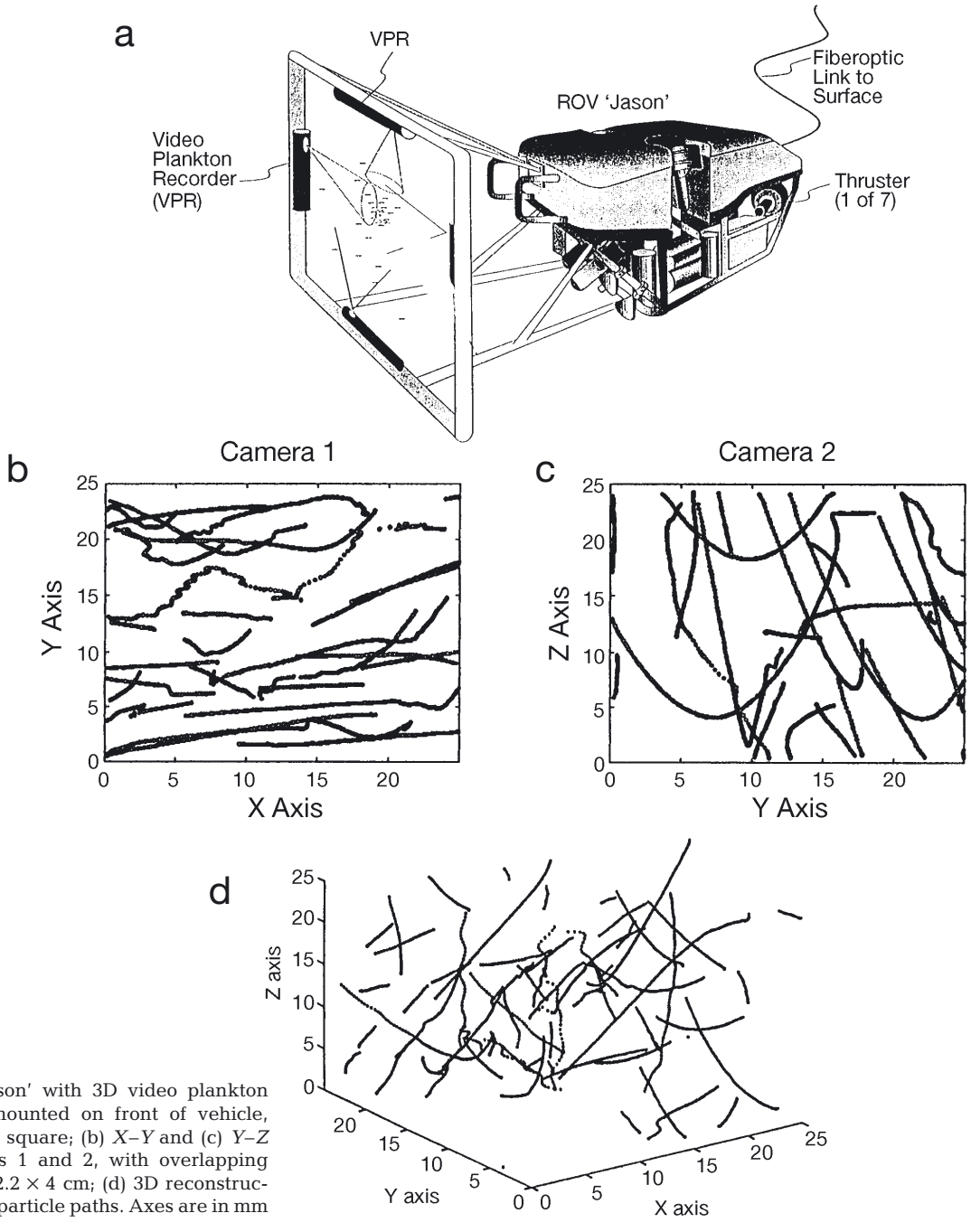

Fig. 3. (a) ROV 'Jason' with 3D video plankton recorder (3DVPR) mounted on front of vehicle, camera frame is 2 m square; (b) X–Y and (c) Y–Z views from Cameras 1 and 2, with overlapping fields of view 2.5 × 2.2 × 4 cm; (d) 3D reconstruction of plankton and particle paths. Axes are in mm

prototcol was to descend to a particular depth, move forward into an undisturbed volume of water, and coast to a stop while maintaining vertical and horizontal position by watching the video displays of the VPR cameras. Recording sequences were limited by the length of the tether to about 3 min, before slack was removed by the ship's motion. Typically, 15 to 30 min were spent at each 5 m depth interval, with intervals extending from the surface to 10 m off the bottom. Video recorders remained active during transition between depth intervals to allow continuous estimates of plankton distributions.

Data processing. Both semi-automated and manual methods of digitizing video signals were used to analyze particle and plankton paths. The semi-automated approach involved digitizing the signals either in real-time (single channel) or from the video-tapes (2 channels digitized sequentially) using a Motion Analysis VP110 image-processor. This system uses a nearest neighbor-algorithm to track the centroids of

particles through time after setting minimum and maximum thresholds for particle luminosity, size, and speed. The ASCII output file, consisting of time x, and location y of particle centroids linked into paths was processed further in Matlab (MathWorks, Cambridge, Massachusetts) using a variety of custom programs. When processing $X–Y$, $Y–Z$ camera signals sequentially, the 1 kHz audio tone, recorded previously on the tapes, was used to trigger the processor to begin digitizing a video sequence, thus affording field-accurate time-matching of stereo sequences.

Although the VP110 allowed bulk-tracking of thousands of particles during each 2 to 3 min video segment that was useful for statistical purposes, it did not allow individual identification of particles and their associated paths. To obtain data on individual identified plankton, a custom package for manually tracking was developed using Matlab. A user would typically advance the video-tape recorder field by field and use a mouse to click on the center of a target identified sequentially through time. $X–Y$ and $Y–Z$ video-tapes were processed sequentially, and the data were merged using time as an index. Position, component velocities, speed, and a variety of statistical parameters were used to characterize each path. Both actively swimming plankton and passive particles which appeared to follow the average flow field were digitized. This allowed a statistical evaluation of the best approach for separating plankton paths from those of passive particles automatically, through bulk analysis with the VP110.

Particle tracks from the VP110 were subjected to statistical analyses for parameterization of turbulence and plankton swimming speeds. First, the $X–Y$ and $Y–Z$ data for each path were merged using time as an index. To determine error associated with the digitization and merging processes, and to correct for misalignment and registration of the image volumes, the Y data common to both views were regressed in a least-squares manner and the slopes used to interpolate a correction factor. A correction was calculated for each deployment, since some adjustments to the optical system were made during the cruise; r^2 values were always significant to the 0.001 level. Next, a matrix of 3D particle positions over time for each path was assembled, followed by calculations of displacement and velocity (u, v, w) in each of 3 directions, x, y, z. To remove the effect of common mode motion due to positioning the ROV, the time-dependent average velocity of the ensemble was calculated between each video field as:

$$U_x = \sum u/N \qquad U_y = \sum v/N, \qquad U_z = \sum w/N \tag{2}$$

where N is the number of particles in a field. U_x, U_y and U_z were subtracted from each path at each time interval to produce background corrected velocities u_c, v_c, w_c along each path:

$$u_c = u - U_x \qquad v_c = v - U_y \qquad w_c = w - U_z \tag{3}$$

Mean ($\overline{u}_c$, $\overline{v}_c$, $\overline{w}_c$) and root mean-square (rms) fluctuating (u', v', w') components of the Lagrangian velocity along the length of each path were calculated respectively as:

$$\overline{u}_c = \sum u_c/n \quad \overline{v}_c = \sum v_c/n \quad \overline{w}_c = \sum w_c/n \tag{4}$$

where n is the number of observations within a path, and:

$$\begin{aligned} u' &= \sqrt{\sum (u_c - \overline{u}_c)^2/n} \\ v' &= \sqrt{\sum (v_c - \overline{v}_c)^2/n} \\ w' &= \sqrt{\sum (w_c - \overline{w}_c)^2/n} \end{aligned} \tag{5}$$

The 3-component turbulence velocity, q (m s^{-1}), was calculated by:

$$q = \sqrt{(u')^2 + (v')^2 + (w')^2} \tag{6}$$

The Lagrangian integral time scale F(s) was estimated by integrating the autocorrelation $c(\Delta t)$ of q along each path up to the first zero crossing:

$$F = \int c(\Delta t)\, d\Delta t \tag{7}$$

The Lagrangian integral length scale (m) was defined as $l_L = q\int F$ (Tennekes & Lumley 1972). Finally, the energy dissipation rate ε (W kg^{-1}) for a given path was estimated by:

$$\varepsilon = Aq^3/l_L \tag{8}$$

where A is a nondimensional constant of the order 1 (Kundu 1990, Moum 1996). ε was ensemble-averaged across particle paths at a bin width of 1 s.

For comparison with rms fluctuating velocities of passive particles following flow, the ensemble-averaged speed for all plankton was calculated as:

$$U_e = \sqrt{(u_c^2 + v_c^2 + w_c^2)} \tag{9}$$

and the average speed U along a given plankton path was calculated as:

$$U_a = \sqrt{(\overline{u}_c^2 + \overline{v}_c^2 + \overline{w}_c^2)} \tag{10}$$

Separation of motile plankton. It was necessary to develop a statistic that would allow separation of active plankton from passive particles based on data obtained through manual analysis, which could later be applied to the semi-automated analyses. To accomplish this, 450 particles and plankton were tracked manually under a variety of environmental conditions. Plankton which could be identified manually because of their shape or motion were categorized separately from particles which tended to follow general flow through the image volume. Acceleration was calculated for passive particles and plankton and compared

through computation of a coherence function (C_{qs}) which is the magnitude-squared coherence between particle and plankton accelerations:

$$C_{qs} = P_{qs}^2/(P_{qq}P_{ss}) \quad (11)$$

where P_{qq} is the power spectrum magnitude for particle acceleration, P_{ss} is the power spectrum magnitude for plankton acceleration, and P_{qs} is the cross-spectral density between P_{qq} and P_{ss}.

Plankton and particle distributions. Fine-scale and microscale vertical distribution of plankton in relation to physical structure of the water column were obtained as ROV 'Jason' descended and ascended between depths. Zooplankton, phytoplankton, and passive particles were grouped into categories depending on how they appeared in the 3DVPR images. Samples obtained by water-bottle casts were examined to help establish these categories and to confirm identifications. Phytoplankton categories included rod-shaped diatoms, the colonial diatoms *Chaetoceros socialis*, a large amorphous mass of cells, and *C. debilis*, a corkscrew-shaped chain diatom. The dinoflagellate *Ceratium* sp. was identified by virtue of its unique anchor shape. Zooplankton categories included juvenile and adult stages of the copepods *Calanus* sp., and *Pseudocalanus* sp., copepods other than these 2 species, and all copepod nauplii. Taxa observed clearly in the VPR images but not included here (since they were relatively rare) were larvaceans, hydroids, pteropods, chaetognaths, and a variety of lesser taxa.

Plankton concentrations were calculated from numbers of a given taxon imaged per unit volume multiplied by the sampling frequency ($60\ \text{Hz} \times 231\ \text{cm}^3 = 13.9\ \text{l s}^{-1}$). Individual observations of plankton were time-matched with depths and ROV translational speeds were interpolated from the CTD record and then binned at intervals of 5 cm in the vertical domain. These data were used directly for estimates of aggregation at the microscale, while fine-scale distributions were prepared by averaging over 1 m intervals. Care was taken not to make multiple identifications of the same individual, since ROV speeds were less than the imaging rate of the cameras.

To identify where plankton and particles had accumulated into well-defined layers, a peak in the fine-scale vertical distribution of a given particle type with respect to depth was defined as the local maximum at which the preceding concentration gradient (dp/dz), where p is the concentration of a particular particle type, exceeded 50% of the maximum gradient observed for that plankton or particle type. Correlative relationships for local maxima or peaks identified in this way and hydrographic and physical variables (salinity, N^2, Ri) were identified.

A plankton aggregation index (Ag) was used to evaluate the microscale (<1 m) distribution independently of total plankton abundance using a point-process similar to that described by Gallager et al. (1996b). At each depth where behavioral observations were made along a given transect, the horizontal distribution of each plankton group was processed using a sliding 1 m window centered on each individual. N represents the total number of individuals of a particular group in a transect with length L, and N_i is the number of individuals within 1 m of each ith individual along that transect (i = 1, 2, 3..., N). Under randomness, the expected value of N_i is $2(N-1)/L$. Ag, then, is defined as:

$$\text{Ag} = (\sum N_i/N) \,/\, \left[2(N-1)/L\right] \quad (12)$$

where the sum is over N individuals within a transect. The significance of Ag was determined by a simple simulation procedure, whereby Ag was calculated for each of 100 random distributions of N individuals along a simulated transect of length L. The measured distribution was significantly uniform or aggregated if the observed value of Ag was below the lower 0.05 quantile or above the upper 0.05 quantile of the distribution of Ag, respectively.

RESULTS

Hydrography

The CTD sensors on ROV 'Jason' indicated a stratified water column with an upper mixed layer above 10 m; 4 broad regions of strong temperature transition were evident: 10 to 13, 22 to 30, 35 to 38, and 45 to 48 m (Fig. 4). Salinity increased from 32.5 near surface to 32.85 at 50 m. Within these broad regions of transition, the local density profile contained 5 prominent shoulders at depths of 12.4, 25.3, 29.5, 37.3 and 46.9 m. With the exception of the shoulder at 46.9 m, density discontinuities were mainly a result of a decrease in temperature, since salinity changed relatively slowly with depth. The N^2 profile reflected density discontinuities and exceeded moderate ($1.25 \times 10^{-4}\ \text{s}^{-2}$) to high ($2.50 \times 10^{-4}\ \text{s}^{-2}$) values at the same 5 depths. The ADCP allowed calculations of shear below a depth of 15 m. With the exception of the peak at 48 m, shear maxima with peak values $>0.045\ \text{s}^{-1}$ were coincident with low N^2, while shear minima $<0.03\ \text{s}^{-1}$ tended to occur where N^2 was greatest. Ri numbers less than 1 were typically associated with high shear. Regions of high water column stability, Ri >1, were between 22 to 30 m and 35 to 39 m. Although Ri numbers could not be calculated without estimates of shear above 15 m, very high N^2 values at 12 m indicate a region of strong density stratification, and perhaps low mixing rates.

A strong fluorescence maximum occurred between 30 and 40 m with a peak at 32 m. Although the peak

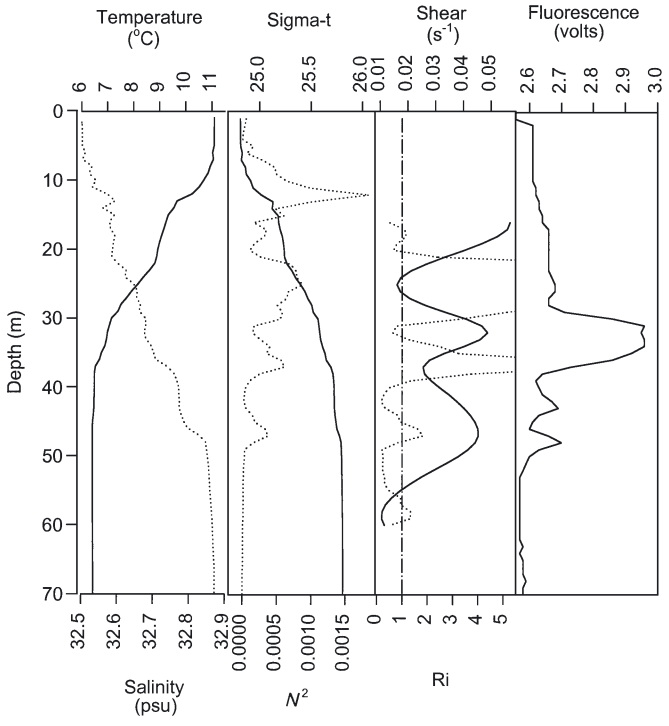

Fig. 4. Hydrographic and physical characteristics of water column during ROV 'Jason' deployment: temperature (—), salinity (·····), sigma-*t* (—), Brunt-Vaisala frequency N^2 (·····); vertical shear (—); Richardson number Ri (·····); Ri = 1 (·–·); and fluorescence (—)

was centered on a region of high shear, low N^2, and Ri <1, a strong fluorescence signal extended deep into the region of high stability.

Plankton and particle distributions

The vertical distribution and abundance of plankton and particles as a function of depth were highly variable, with multiple peaks and troughs (Fig. 5). Most groups were found in layers ranging from 5 cm to 10 m in thickness, while others such as *Chaetoceros socialis* formed broad distributions 20 to 30 m thick and exceeded a concentration of 250 colonies l^{-1}.

We identified 2 to 6 peaks for each particle type, and compared these with the corresponding values for N^2 and Ri (Fig. 6). The location of each peak in particle abundance was then associated with its nearest local N^2 maxima or minima (Table 1). Marine snow formed maximum abundances at 6 locations in the water column, reaching a maximum concentration of 3.8 particles l^{-1} at a depth of 42.3 m (Fig. 5). Although peak abundances occurred in close association with maximum values of N^2 at 3 depths (11.9, 24.8, 47.4 m), peaks also occurred at depths where the density gradient was least (20.2, 34.7, 42.3 m); 2 of these peaks were located where Ri was below 1.25 (20.2 and 42.3 m), while the peak located at 34.7 m was associated with a Ri number of 3.00 (Table 1). The physical conditions at a depth of 34 m indicated a series of density folds, resulting in the formation of layers on the order of 10 to 50 cm in thickness. Marine snow along with all other

Table 1. Peak locations of plankton and particles relative to hydrographic condition. N^2: Brunt-Vaisala frequency; Ri: Richardson numbers

Depth at peak location (m)	Corresponding N^2 ($\times 10^{-3}$)	Ri	Peak location relative to local N^2 maxima (m)
Marine snow			
11.9	1.75	–	−0.1
20.2	0.14	1.02	+0.2
24.8	0.85	32.00	−0.2
34.7	0.36	3.00	−0.3
42.3	0.03	0.23	+0.3
47.4	0.29	1.43	+0.4
Chaetoceros socialis			
11.7	1.58	–	−0.3
34.5	0.37	2.86	−0.5
39.1	0.10	1.27	−2.9
47.9	0.18	0.93	+0.9
Chaetoceros debilis			
42.4	0.10	0.25	+0.4
43.5	0.03	0.58	+1.4
48.4	0.06	0.33	−2.6
Rod diatoms			
13.8	0.58	–	−0.2
34.1	0.39	2.57	+0.1
42.8	0.05	0.31	+0.8
49.7	0.03	0.24	−1.3
Ceratium sp.			
11.5	1.40	—	−0.5
34.1	0.39	2.57	+0.1
38.7	0.15	0.31	+1.7
40.9	0.03	2.06	−1.1
Unidentified copepods			
7.4	0.36	–	+0.5
16.1	0.18	0.57	+0.1
34.0	0.40	2.50	0
38.7	0.15	2.07	+1.7
48.8	0.06	0.33	+2.0
Copepod nauplii			
12.4	1.50	–	+0.4
19.8	0.12	0.69	−0.2
33.6	0.34	2.01	−0.3
42.8	0.05	0.31	+0.8
47.4	0.29	1.43	+0.4
Pseudocalanus sp.			
42.8	0.05	0.31	+0.8
49.3	0.03	0.22	+0.7
Calanus sp.			
7.0	0.29	–	+0.2
16.4	0.23	0.75	+0.4
21.6	0.52	6.82	+1.6
33.8	0.37	2.26	−0.2
38.1	0.24	3.45	+1.1
44.6	0.17	0.89	+2.6

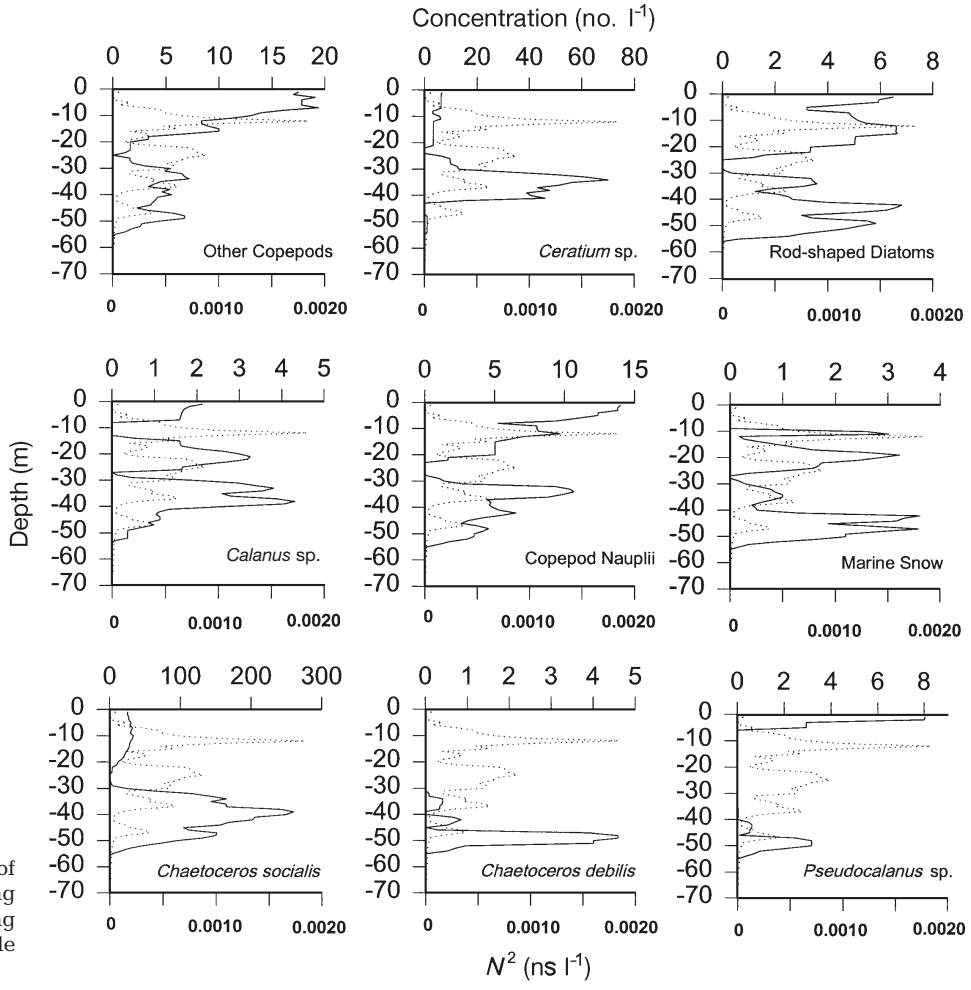

Fig. 5. Vertical distribution of plankton and particles during ROV deployment (—), showing concentration and depth profile of N^2 (·····)

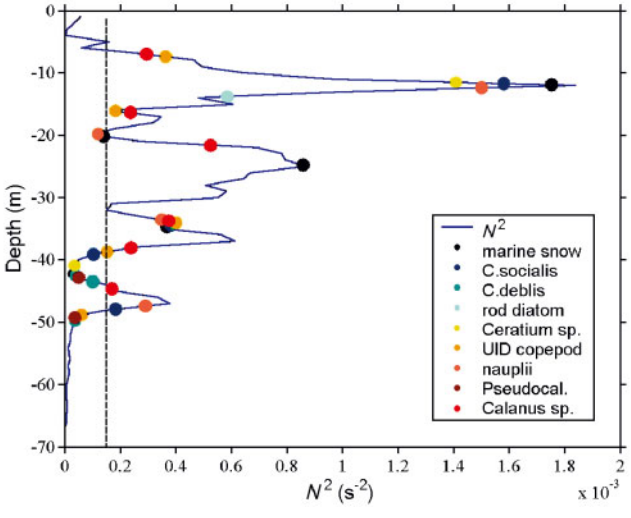

Fig. 6. Vertical distribution of peak abundances of plankton and particle. Taxa or particle type shown in color (see key). Peaks were identified where local maxima of dp/dz exceeded 50% of the maximum gradient for that plankton or particle type. Full specific names are given in Table 1. UID: unidentified copepods

particles and plankton, with the exception of *Pseudocalanus* sp., exhibited local maxima within these folds. Multiple peaks in snow abundance at 42.3 and 47.4 m were associated with a region of unstable water (Ri = 0.23) overlying a relatively strong density gradient (N^2 = 2.9 × 10^{-4} s^{-2}, Table 1). This layering affect of abundance peaks associated with unstable water overlying stable water also occurred at 20.2 and 24.8 m. The peak located at 11.9 m was centered on a high value of N^2, but appeared not to be associated with overlying unstable water.

The colonial diatom *Chaetoceros socialis* had a distribution similar to that of marine snow (Figs. 5 & 6), with extreme concentrations exceeding 250 colonies l^{-1}. Peak abundances were located in direct association with high N^2 values at depths of 11.7, 34.5, and 47.9 m. However, the abundance peak at 39.1 m, which overlaid another peak at 47.9 m, corresponded to relatively low N^2 and Ri values.

Another diatom, *Chaetoceros debilis*, reached a maximum concentration of 4.5 chains l^{-1} at a depth of

48.4 m. Rod-shaped diatoms were distributed in a pattern similar to marine snow, reaching a concentration of 6.5 chains l^{-1}. *Ceratium* sp. was distributed between 30 and 40 m, with a sharp peak at 34.1 m.

Calanus sp. and unidentified copepods were grouped similarly in regions where N^2 values were increasing rapidly rather than where the density gradient was at a maximum or minimum. Nevertheless, dense accumulations of copepods generally occurred at N^2 values above 1.25×10^{-4} s^{-2}. Since N^2 typically increased from minima to maxima over a depth of 4 to 5 m, peak abundances of most copepods were observed about 2 m above maximum values of N^2. An exception to this was observed at a depth of 38.1 m, where *Calanus* sp. aggregated at densities exceeding 4 l^{-1} while the density gradient was decreasing rather than increasing. Therefore, *Calanus* sp. aggregations formed both above and below the depth where N^2 was maximum.

Copepod nauplii exhibited a distributional pattern nearly identical to that of marine snow, with the exception of a peak at 24.8 m and an elevated near-surface abundance.

Pseudocalanus sp. was located only in regions where N^2 values were well below 1.25×10^{-4} s^{-2}: above and below the density gradient maxima at 47.0 m and near the surface.

Separation of plankton and particles

To allow for automatic identification of paths produced by passive particles following flow and those of motile organisms swimming through the field, a series of paths were separated by hand while observing particle motion on the video monitor. Background-corrected plots of *ZX* coordinates over time indicated that plankton-generated paths were more circuitous than those of coincident particle paths, and the net to gross displacement ratio (NGDR) was significantly different between groups (Student's *t*-test, $p < 0.01$, Table 2). Although the mean speed of background-corrected plankton paths was considerably lower than the mean passive particle speed (as would be expected under turbulent conditions) mean acceleration calculated along the length of a given path for plankton was 2 to 100 times greater than that of passive particles (Fig. 7; Table 2). This suggests that acceleration rather than speed was a more sensitive indicator of passive versus active targets.

Coherence of acceleration between motile plankton and passive particles tracked by hand was high at frequencies below 3 Hz, falling to less than 0.2 at 10 Hz (Fig. 8). Thus, acceleration along paths generated by plankton and particles was similar at low frequencies but diverged at frequencies greater than ~10 Hz; however, coherence between the motion of a passive particle and background flow was always above 0.5 up to a frequency of 15 Hz. A threshold was set, therefore, at 0.2 and 10 Hz, distinguishing motile plankton from the movement of passive particles. For example, if coherence between the acceleration of a path and the ensemble-averaged background particle acceleration during the same time interval was greater than 0.2 at a frequency of 10 Hz, the path was labeled as a passive particle.

Following the separation of paths into active and passive categories, plankton swimming speeds (U_e) were compared with the 3-component turbulence velocity q and energy dissipation ε. Fig. 9a illustrates the comparison for plankton swimming speeds U_e and q sampled at a depth of 36 m, just 1 m above a local maximum in the density gradient. In this region of high stability, q remained <1 mm s^{-1} for most of the 30 s sampling intervals. Occasional spikes at apparently random intervals of about 4 to 8 s increased background flow to >2 mm s^{-1}. Plankton swimming speeds over the same time interval were 3 to 10 times greater than q. In contrast, at a depth of 50 m (Fig. 9b), where water-column stability was low, values for q exceeded 3 mm s^{-1} on average and periodically exceeded 10 mm s^{-1}. U_e remained about 2.5 times lower than q throughout the 43 s sampling interval.

Table 2. Criteria for manually identifying and separating particle tracks. Data are means (SD). NGDR: net to gross displacement of an organism along its motion path

Organism	Speed (mm s^{-1})	Acceleration (mm s^{-2})	NGDR
Copepods	6.3	78.7	0.47
	16.1	514.1	0.05
	40.5	524.2	0.84
	5.3	100.6	0.26
	15.2	370.1	0.83
	18.9	228.1	0.28
	15.7	289.6	0.54
	30.5	508.5	0.98
Protozoans	4.7	15.4	0.37
	9.7	41.8	0.92
	12.0	27.2	0.96
	10.3	129.0	0.83
	10.8	73.4	0.89
	5.3	56.2	0.98
	4.9	48.5	0.78
	5.3	60.9	0.25
	11.4	174.3	0.96
	9.2	54.1	0.62
All swimming plankton	12.9 (9.4)	183.1 (180.0)	0.66 (0.31)
All passive particles	92.8 (82.8)	72.0 (61.3)	0.87 (0.26)

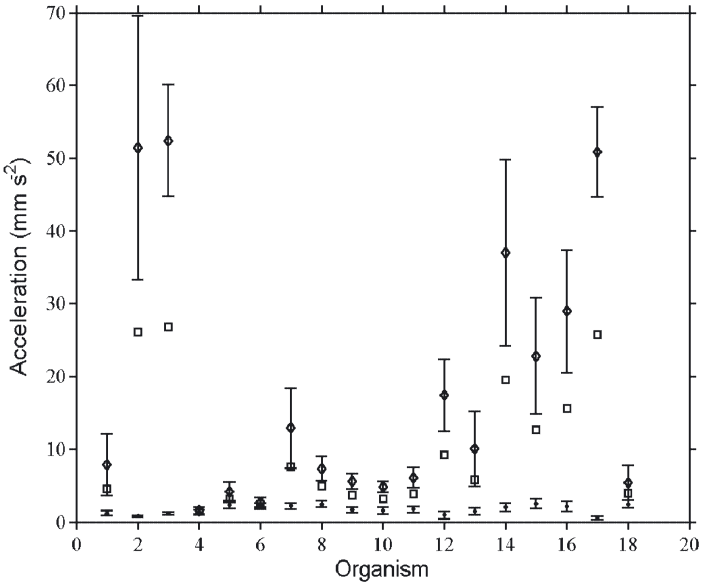

Fig. 7. Kinematic characteristics of motile and non-motile particles identified and separated by hand. Data for plankton (◇) are accelerations along individual paths. Data for particles (•) are ensemble averages of acceleration for all particles during same time window as a particular plankton. Ensemble average (□) was calculated for entire assemblage during the time window in which a particular plankter was in view. Mean ±SD 1–3: copepod; 4–12: protozoan; 13–17: copepod; 18: protozoan

We call the ratio U_a/q the motility number (Mn), which indicates the potential for plankton to swim against uncorrelated turbulence velocities. Values >1 indicate, on average, that plankton swimming speeds were greater than turbulence velocities. The time-course of variation in Mn for the entire plankton community (Fig. 10) indicates the large variation associated with instantaneous changes in swimming speed and q. For paths sampled at 36 m, 95% were produced by plankton with on Mn >1 (Fig. 10a), while at 50 m depth 92% were <1 (Fig. 10b).

Plankton swimming speeds averaged over the duration of each path, U_a, remained remarkably constant with depth regardless of species composition, while q varied by a factor of 20 (Table 3). Energy dissipation rate (ε) was high near the surface and below 40 m (order 10^{-6} to 10^{-7} W kg^{-1}), but relatively low (order 10^{-8} W kg^{-1}) where the density gradient was strong and Ri was relatively high. Mn for all non-motile particles including marine snow, *Chaetoceros socialis*, *C. debilis*, and rod diatoms was between 0.1 and 1.5.

The Ag measured the tendency for distributions to differ from random either in the direction of uniform or aggregated. No distributions were found to be uniformly distributed, whereas some of the motile organisms showed significantly aggregated distributions (Table 3). *Ceratium* sp., nauplii and *Calanus* sp. all showed aggregated distributions at intermediate depths of 33 to 40 m. For *Ceratium*, Ag showed aggregation when Mn exceeded about 3. *Calanus* sp. showed aggregation at Mn greater than 3.3, while nauplii required values of Mn greater than 13 for an aggregation to exist. The Mn for nauplii was considerably higher than for any other plankter because of the near-continuous series of rapid jumps made by this group.

When comparing turbulence intensity with plankton swimming behavior, it is useful to consider the Lagrangian velocity spectra. When the Reynolds number is sufficiently high, the Lagrangian velocity spectra exhibit an inertial subrange as the Eulerian velocity spectrum. The slope for the inertial subrange of the Eulerian spectrum is well known for being –5/3 in terms of either wavenumber, k, or frequency, f, while the Lagrangian velocity spectrum shows f^{-2} (Tennekes & Lumley 1972). At a depth of 36 m, background turbulence produced a velocity spectrum with a slope of –2 up to the Nyquist frequency (30 Hz) (Fig. 11). This was expected, since the corresponding Ozmidov scale at this depth is about 0.08 m, so turbulent eddies exceeding this length scale are not free from the effect of buoyancy. The spectrum for plankton also had a slope of about –2 extending to a frequency of about 19 Hz, but the magnitude was about 10 times that for passive particles. Therefore, the energy spectrum produced by plankton was greater than that generated by turbulence. Conversely, at a depth of 50 m, energy intensity and the slopes for turbulence and plankton were –2 and magnitudes were not significantly different (ANCOVA: $p > 0.05$).

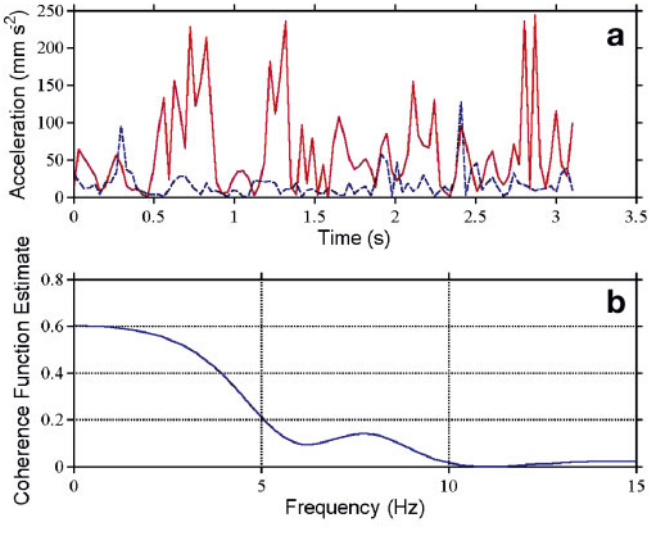

Fig. 8. Statistics for separation of plankton and particles identified by hand. (a) Ensemble average of acceleration of plankton (continuous line) and particles (dashed line); (b) coherence between acceleration of plankton and particles

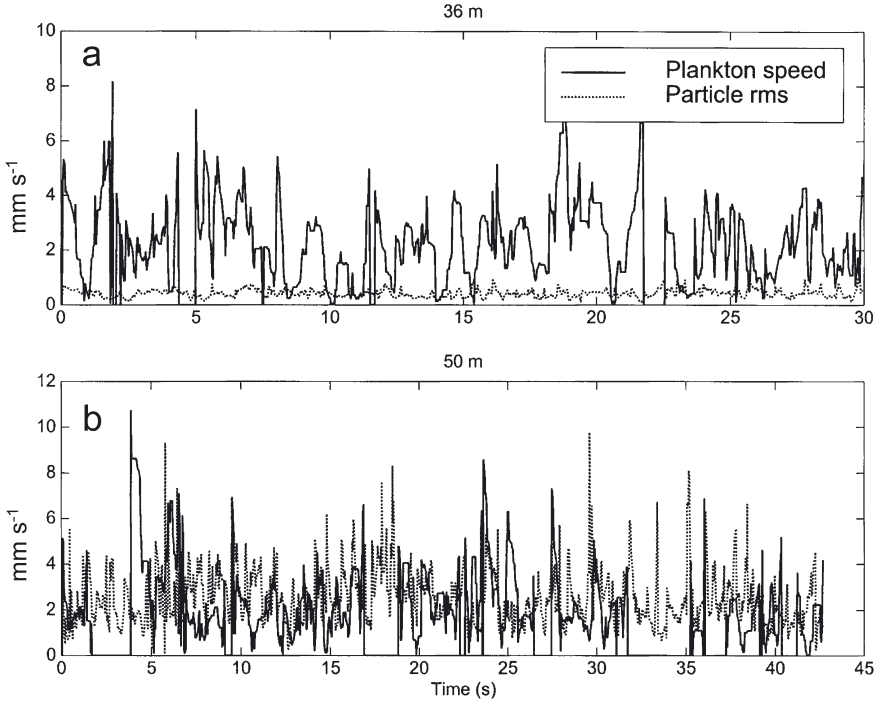

Fig. 9. Example of plankton speed and particle rms speed at (a) 36 and (b) 50 m. Data for plankton and particles were separated using criterion for coherence of acceleration given in 'Materials and methods'

DISCUSSION

Fine-scale vertical distributions of actively swimming plankton and passive particles followed distinctly different patterns. Peaks in marine snow and *Chaetoceros socialis* colonies were just as likely to be found at density gradient maxima as at gradient minima. However, peak abundances for *Calanus* sp. were centered on inflection points in density where N^2 was about 2.5×10^{-4} s^{-2}. Potential mechanisms responsible for these distributions include reduction in sinking velocities with depth due to density stratification, interaction of plankton and particles with turbulence, shear-induced horizontal intrusion of different plankton communities, interaction of internal waves with biological gradients (Franks 1995), and behaviorally directed swimming. It is important to keep in mind that the shear-induced mixing discussed by Eckart (1948) and Osborn (1998) is a mechanism for redistributing horizontal variability, into vertical variability producing the kind of fine-scale

Table 3. Motility characteristics of the plankton community and physical characteristics of the water column. U_a: average velocity; q: turbulence velocity; ε: dissipation; Mn_a: ensemble average motility number; N^2: Brunt-Vaisala frequency; Ri: Richardson number; Snow: marine snow; *C.soc.*: *Chaetoceros socialis*; *C.deb.*: *C. debilis*; Rod: rod diatoms; *Cer*: *Ceratium* sp.; Mn = motility number; Ag = aggregation index; R: random; A: aggregated. U_a, q, and Mn_a are means of the entire plankton and particle assemblage. Mn and Ag are calculated for each taxon separately

Community							Taxon						
Depth (m)	U_a (mm s^{-1})	q (mm s^{-1})	MN_a	ε (W kg^{-1})	$N^2 \times 10^{-4}$ (s^{-2})	Ri	Snow Mn Ag	*C.soc.* Mn Ag	*C.deb.* Mn Ag	Rod Mn Ag	*Cer.* Mn Ag	Nauplii Mn Ag	*Calanus* Mn Ag
20	1.8	5.50	0.3	5.7×10^{-7}	1.1	0.7	0.1 R	0.02 R	0.02 R	0.01 R	0.36 R	4.0 R	1.0 R
20	1.4	4.10	0.3	3.3×10^{-7}	1.1	0.7	0.1 R	0.02 R	0.02 R	0.01 R	0.49 R	5.4 R	1.4 R
33	1.0	0.39	2.6	9.3×10^{-8}	2.7	1.3	1.0 R	0.26 R	0.26 R	0.10 R	5.10 A	56.9 A	14.6 A
34	1.6	0.33	4.8	9.3×10^{-8}	4.0	2.5	1.2 R	0..30 R	0.30 R	0.12 R	6.06 A	67.3 A	17.2 A
36	3.3	0.55	6.0	6.1×10^{-8}	5.6	7.3	0.7 R	0.18 R	0.18 R	0.07 R	3.64 A	40.4 A	10.4 A
36	1.4	0.30	4.7	1.1×10^{-7}	5.6	7.3	1.3 R	0.33 R	0.33 R	0.13 R	6.68 A	74.0 A	19.0 A
36	1.7	0.40	4.3	7.0×10^{-8}	5.6	7.3	1.0 R	0.25 R	0.25 R	0.10 R	5.00 A	55.5 A	14.3 A
36	1.5	0.38	3.9	8.5×10^{-8}	5.6	7.3	1.1 R	0.26 R	0.26 R	0.11 R	5.26 A	58.4 A	15.0 A
38	1.3	0.32	4.1	5.7×10^{-8}	2.5	3.7	1.3 R	0.31 R	0.31 R	0.13 R	6.25 A	69.3 A	17.8 A
40	1.5	0.30	5.0	1.2×10^{-7}	5.0	0.5	1.3 R	0.33 R	0.33 R	0.13 R	6.66 A	74.0 A	19.0 A
50	1.0	1.70	0.6	4.2×10^{-6}	0.4	0.3	0.2 R	0.06 R	0.06 R	0.02 R	1.18 R	13.1 R	3.3 R
50	1.4	2.20	0.6	1.2×10^{-6}	0.4	0.3	0.2 R	0.05 R	0.05 R	0.02 R	0.90 R	10.1 R	2.5 R

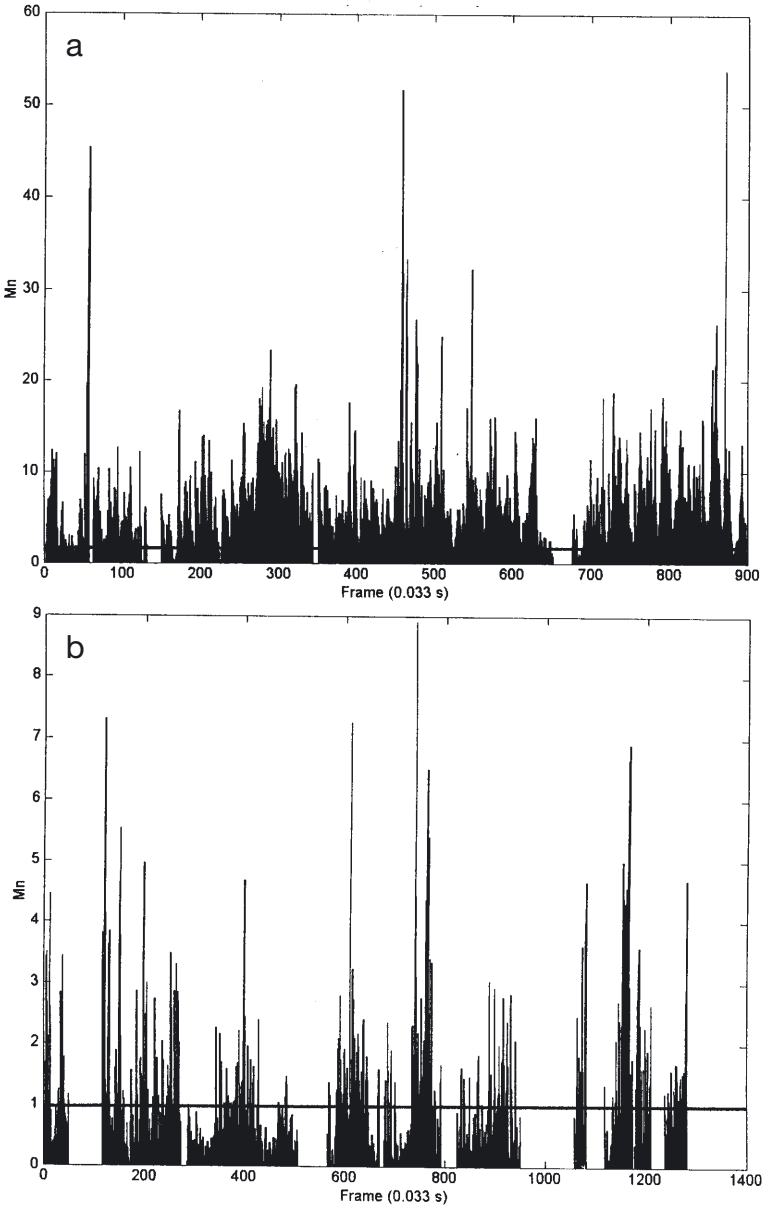

Fig. 10. Time series of motility number, Mn (ratio plankton speed/particle rms) at (a) 36 m and (b) 50 m. Data are given for each 1/30 s interval when plankton were present. Horizontal line indicates Mn = 1

structure typically observed in vertical profiles of physical constituents. This redistribution of water could also result directly in the redistribution of organisms and chemicals into thin layers, if they are associated with the physical gradients to begin with. Alternatively, thin layers in biological and chemical fine-structure could form after physical gradients are produced through mixing. Either way, the primary mechanism of concentration or retention of particulate or biological material relative to average levels would not be shear, but some intrinsic characteristic of the water mass such as density or viscosity. However, shear may be directly responsible for particle aggregation in the turbulent strain field below the Kolmogorov scale (Squires & Yamazaki 1995).

Seasonal changes in density stratification lead to strong physical gradients which could allow accumulation of sinking particles under specific conditions (Lande & Wood 1987, MacIntyre et al. 1995). MacIntyre et al. (1995) calculated that in order for particulate material to be accumulated at a moderately strong density interface of $N^2 > 4 \times 10^{-4}$, sinking speeds must be reduced by >20%. To achieve this change in sinking speed, particles must be large (>1 mm in diameter), have a high porosity (>99%), and low interstitial equilibration time (min to d). MacIntyre et al. (1995) argued that large marine flocs fitting this description will tend to slow as they encounter a steep density gradient, since interstitial fluid is at a lower density than surrounding fluid and some time is required for its equilibrium. This is particularly true for marine flocs with high mucus content and when the flocs are sinking through a halocline, since heat diffusion is rapid compared with salt diffusion and both are considerably slower through mucus. Colonies of *Chaetoceros socialis* are typically 1 to 2 mm in diameter, hollow, and roughly spherical in shape, and contain large amounts of mucopolysaccarides (Sieracki et al. 1998). Although their sinking velocity has not been measured directly in the laboratory, our estimates from the field are between 0.001 to 0.1 mm s^{-1} or 0.086 to 8.6 m d^{-1}, which is consistent with previous studies on large diatom colonies (Eppley et al. 1967). MacIntyre et al. (1995) showed that the sinking speed of a floc as it falls through a density gradient is dependent on the ratio $\sqrt{\Delta P}$ where the floc was formed, to $\sqrt{\Delta P}$ at the new density. ΔP is the excess density between the floc and the fluid and is dependent on the solid volume fraction and porosity. If we use 0.01 g cm^{-3} for excess density and a porosity of 99.9%, which is consistent with a floc with a diameter of 2 to 10 mm (Alldridge & Gotschalk 1988), the percentage change in sinking speed may be calculated using the equations presented in MacIntyre et al. (1995). We find that with a modest change in density of only 0.02 g cm^{-3} over 1 m, $N^2 = 2 \times 10^{-4}$ s^{-2}, colony sinking-speed may virtually drop to zero. This appears as a plausible explanation for the intense accumulations of *C. socialis* immediately above the pycnocline associated with a 'cold pool' (Houghton et al. 1982) of shelf water. Such accu-

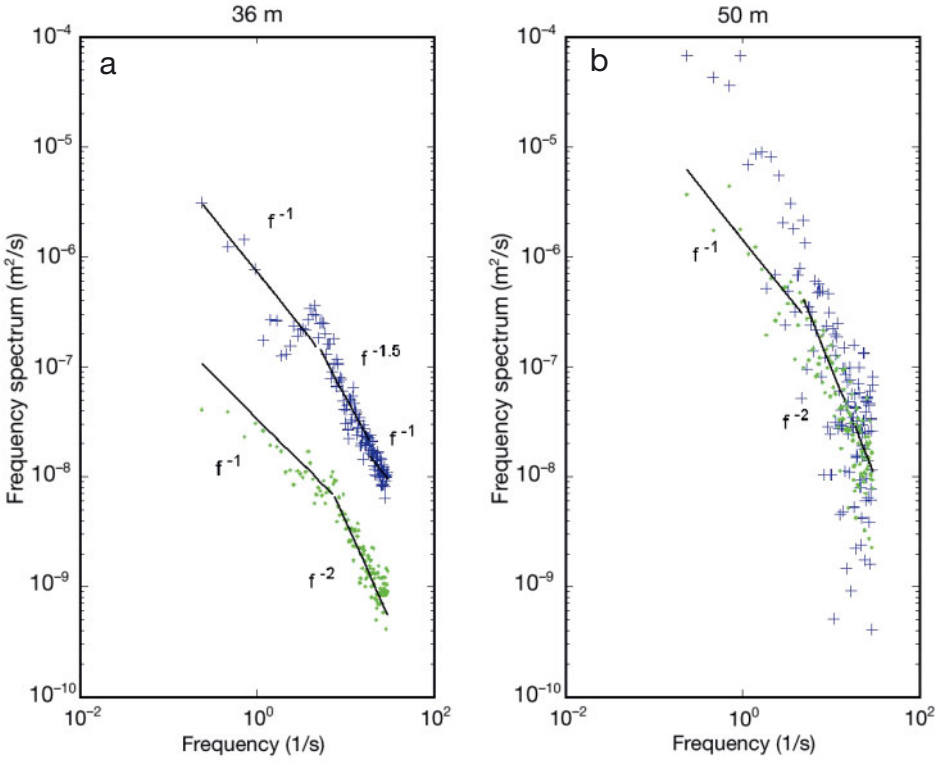

11. Lagrangian velocity spectra for plankton and particles at (a) 36 m and (b) 50 m. *f*: frequency; +: plankton; ●: particles

mulations have been observed on the Southern Flank of Georges Bank by Bigelow (1924) and Sieracki et al. (1998), and in the Great South Channel by Gallager et al. (1996b).

Both *Chaetoceros socialis* and marine snow concentrations were elevated between depths of 30 and 50 m, and both groups had 3 distinct peaks within this 20 m range. Marine snow had peak abundances at 34.7, 42.3, and 47.4 m with only the first and last peak being associated with N^2 values greater than 1.25×10^{-4} s^{-2}. *C. socialis* had a distribution similar to this, with the exception of the central peak being 3 m shallower and closer to the N^2 maxima. This region appears to be a prime example of shear-induced thin-layering as described by Eckart (1948) and, more recently, by Osborn (1998). By stretching a parcel of fluid horizontally, the thickness of the parcel decreases and the vertical gradient relative to background increases. Moreover, multiple thin-layers meters in thickness can result as horizontal patches are stretched to the extent that they overlap vertically. When a profile is made by some instrument from the surface, these overlapping parcels are viewed as thin layers in a typical 2 dimensional plot of concentration versus depth.

High shear above and below a region of relatively high stability (e.g. 34 to 38 m) is consistent with Eckart's (1948) thesis. The highly stable region in the center could be the source population for the immediately adjacent upper and lower peaks. This does not preclude the possibility that *C. socialis* was actively growing under these conditions and that marine snow was actively forming. Although we do not know if growth was occurring, on the same cruise, Sieracki et al. (1998) observed that *C. socialis* colonies at 30 m were located above the 1% light level, while the individual cells were intact and appeared healthy, suggesting that growth was likely.

Another region of accumulation of both marine snow and *Chaetoceros socialis* was at 12 m. Small changes in salinity relative to large vertical gradients in temperature at 12 m suggest that the large Brunt-Vaisala frequencies ($N^2 = 15.4 \times 10^{-4}$ s^{-2}) observed at this depth are due to thermal stratification rather than intrusion of different water masses. Observed distributions of *Chaetoceros socialis* and marine snow at 12 m are consistent with the explanation of particle accumulation at a density interface.

The distribution of *Calanus* sp. was similar to that of marine snow and *Chaetoceros socialis* at depths of 33, 38 and 44 m, but dissimilar at 7, 16 and 21 m. In both deep and shallow regions, peaks in *Calanus* sp. abundance occurred as the density gradient was increasing or decreasing, and was never centered on a N^2 maximum or minimum. In addition, *Calanus* sp. were aggregated wherever the turbulent rms velocity was below ~0.5 mm s^{-1} on either side of a density maximum. One explanation for this distribution lies in Eckart's (1948) description of layering. If *Calanus* sp.

formed an abundance peak centered on a density gradient maximum, vertical shear could redistribute the single peak into 3 distinct peaks, 1 above, 1 below, and 1 remaining centered on the density maximum. However, this mechanism does not appear likely, since a peak centered on a density maximum was not seen at any depth. Alternatively, *Calanus* sp. may be sinking through the water column and accumulating at a density interface. Shear immediately above that interface could resuspend organisms causing locally elevated concentrations. However, again, for this explanation we would expect to see 2 maxima, one within the density maximum and another immediately above it.

For *Calanus* sp. and nauplii categories, the most likely explanation for the occurrence of concentration maxima immediately above and below density maxima is swimming behavior. These local concentrations only occurred where *Calanus* sp. swimming speed was at least 10 times higher than rms turbulence velocity. Since significant aggregation occurred only in this same region, *Calanus* sp. must be capable of swimming independently of local turbulent flow. Nauplii were also aggregated where Mn was considerably greater than 1.

Even for the weakly swimming dinoflagellate *Ceratium* sp., populations were significantly aggregated where Mn was ~3 or greater. Formation of layers and streaks of dinoflagellates are well documented in the literature (e.g. Anderson 1997), and appear to occur under highly stratified conditions when mixing in the surface waters is minimal. Swimming speeds noted for dinoflagellates by Levandowsky & Kaneta (1987) and Fraga et al. (1988) suggest that averages of 2 to 3 mm s^{-1} are reasonable for single cells. This would require values of q to be <0.6 mm s^{-1} to allow cells to aggregate relative to turbulent flow, assuming a critical threshold of 3 for Mn. Energy dissipation rates in the seasonal thermocline range between 10^{-10} and 10^{-6} W kg^{-1}, with corresponding rms turbulence velocities ranging between 0.01 and 4 mm s^{-1} (Yamazaki & Squires 1996). A value for q of 0.6 represents a corresponding dissipation rate of about 10^{-8} to 10^{-7} W kg^{-1}, a rate that is common in the pycnocline and during windless days at the surface.

The theory of homogenous, isotropic turbulence predicts that energy dissipation within the inertial subrange of the Eulerian spectrum (stationary frame of reference) decrease with increasing wavenumber, $k^{-5/3}$, or frequency, $f^{-5/3}$ while in the Lagraigian spectrum (moving frame of reference), k^{-2} and f^{-2} (Tennekes & Lumley 1972). In this study, use of the Lagraigian spectrum is appropriate since the frame of reference moved with displacement of each particle tracked by the imaging system. There are always 2 components to the motion of plankton: physical motion generated by local-scale turbulence and swimming motion due to behavior. When the variance spectrum for plankton motion exceeds the variance spectrum for turbulence at a corresponding wave-number, we conclude that plankton are moving independently of turbulence velocity structure. Such is the case for the plankton community shown in Fig. 11 at a depth of 36 m. In this region, N^2 was high and shear was low, leading to an Ri number of 5.6 (Table 3). Measured dissipation rates were on the order of 10^{-8} to 10^{-7} W kg^{-1}, rates typical of a highly stable, strongly stratified pycnocline. The energy spectrum for the motion of plankton and of small particles was close to f^{-2}, while the magnitude for plankton was nearly 10 times higher than for particles. At a depth of 50 m, however, the magnitude and energy dissipation rate for both plankton and particles were comparable, suggesting that plankton were not capable of swimming independently of local flow.

Copepod swimming speeds vary considerably with behavior. During cruising, speeds tend to range from the relatively slow *Acartia tonsa* of 2.5 mm s^{-1} (Buskey et al. 1986) and *Pseudocalanus minutus* of 4 mm s^{-1} (Buskey et al. 1987) to the very fast *Calanus finmarchicus* of 15 mm s^{-1} (Hardy & Bainbridge 1954). Jump and escape sequences are associated with speeds 10 times faster, but are generally not sustained for more than 1 s. Because of artificial boundary conditions and fluid flow, the frequency of jumps and escapes observed in the laboratory may be far greater than is usual *in situ*. Nevertheless, if only cruising speed is compared with rms turbulence velocity, only under the most energetic conditions near the surface during periods of moderate to high wind, or near the benthic bottom layer, would copepods not be capable of swimming against local turbulent flow. The term 'local' is crucial to our interpretation of plankton being passively moved about as a function of water motion since this is a dynamic, anisotropic and scale-dependent process.

Emerging evidence indicates that copepods use a variety of sensory modalities such as mechanical (van Duren et al. 1998, Yen et al. 1998), chemical (Strickler 1998, Weissburg et al. 1998) and light gradients (Ambler et al. 1991) to improve conspecific contact rates (Tsuda & Miller 1998) and for locating prey (Tiselius et al. 1993). Plankton can become concentrated at a variety of interfaces such as at a pycnocline (Mackas et al. 1985), benthic boundary layer, or air-water interface (Gallager et al. 1996), and may become locally enhanced in regions where flow is unidirectional for some period of time, such as in convergent fronts (Alldredge et al. 1984, Beardsley et al. 1996), Langmuir cells (Pollard 1997), and internal waves and bores (Pineda 1991, Shanks et al. 2000). While the motivation for such behavior is still under investiga-

tion, it is clear that physical characteristics of the water column routinely allow biologically-mediated motion to dominate at one scale or another.

Our calculation of Mn suggests that a minimum value of about 3 is necessary for organisms to move independently of local flow. The reason why this values is not 1, relates to the issue of sampling scale. At the level of the individual, swimming plankton will be independent of flow only if (on average) their swimming speed is greater than rms turbulence velocity. Although our averaging periods (i.e. tens of seconds) are reasonable for eddies on the scale of millimeters to centimeters, with time constants of seconds, they are relatively short compared with eddies on the scale of meters and tens of meters, which operate on time scales of minutes. The result is an overestimate of the swimming speed required to become independent of flow. Longer observational times of aggregations or groups of plankton is strictly a technical problem which requires further research.

Our analysis of the contribution of physical processes and biological behavior to the formation of plankton layers illustrates the need to measure both characteristics simultaneously and at the same scale. While vertical shear may not be directly responsible for the concentration of plankton and particles against average background levels, shear can redistribute horizontal patchiness into vertical layers. The primary mechanisms for concentration, then, are gradients in hydrographic characteristics of the water such as density and viscosity, and biological concentration due to swimming behavior, which is in a dynamic balance with turbulence. Passive particles decrease sinking speed at sharp density gradients, but can then be redistributed vertically through mixing at gradient interfaces. Plankton attempting to swim against local velocity structure may rest passively in turbulent conditions until the water column becomes quiescent, or take advantage of transient turbulent-flow structures to augment swimming. However, the fact that the velocity spectra for swimming plankton and passive particles were indistinguishable under turbulent conditions (50 m depth), suggests that plankton become less active when turbulence is elevated. Theoretical (Rothschild & Osborn 1988, Hill et al. 1992) and laboratory (Costello et al. 1990, Saiz 1994) studies on the interaction between copepods and turbulence support the idea that turbulence may passively increase contact rates between predator and prey, thereby allowing the predator to conserve energy. Further *in situ* observations are required to characterize the local environment of plankton for comparison with laboratory studies.

Layering of phytoplankton and zooplankton in the ocean as a function of density discontinuities and behavior will impact primary and secondary production in as yet unknown ways (Cowles et al. 1998). Therefore, it is crucial that the micro- and fine-scale vertical distributions of plankton be measured at the same scales as the prevailing hydrography, and that mechanisms governing the layering process be understood. Direct observation and *in situ* experimentation will allow elucidation of these mechanisms which are undoubtedly organism- and environment-specific.

Acknowledgements. Support for this research was provided by the National Science Foundation, Biological Oceanography, grants OCE-9632596 (C.S.D.) and OCE-9313680 (S.M.G.) and by a Monbusho Grant-in-Aid for Scientific Research (C) 10045026 (H.Y.). We thank the WHOI Deep Submergence Group for their contributions using ROV 'Jason', the crew of the RV 'Endeavor' for help during the GLOBEC field seasons, and Philip Alatalo and Andy Girard for their technical assistance. Contribution #10291 from the Woods Hole Oceanographic Institution and #246 from the US GLOBEC Northwest Atlantic Program.

LITERATURE CITED

Alldredge AL, Gotschalk C (1988) *In situ* settling behavior of marine snow. Limnol Oceanogr 33:339–351

Alldredge AL, Robison B, Fleminger A, Torres J, King J, Hamner W (1984) Direct sampling and *in situ* observation of a persistent copepod aggregation in the mesopelagic zone of the Santa Barbara Basin. Mar Biol 80:75–81

Ambler JW, Ferrari FD, Fornshell JA (1991) Population structure and swarm formation of the cyclopoid copepod *Dioithona oculata* near mangrove cays. J Plankton Res 13: 1257–1272

Anderson DM (1997) Turning back the harmful red tide. Nature 388:513–514

Beardsley RC, Epstein AW, Chen C, Wishner KF, Macaulay MC, Kenney RD (1996) Spatial variability in zooplankton abundance near feeding right whales in the Great South Channel. Deep-Sea Res Part II Top Stud Oceanogr 43: 1601–1625

Bigelow HB (1924) Plankton of the offshore waters of the Gulf of Maine. Bull Bur Fish Wash 40:1–509

Buskey EJ, Mann CG, Swift E (1986) The shadow response of the estuarine copepod *Acartia tonsa* (Dana). J Exp Mar Biol Ecol 103:65–75

Buskey EJ, Mann CG, Swift E (1987) Photophobic responses of calanoid copepods: possible adaptive value. J Plankton Res 9:857–870

Costello JH, Strickler JR, Marrase C, Trager G, Zeller R, Freise AJ (1990) Grazing in a turbulent environment: behavioral response of a calanoid copepod *Centropages hamatus*. Proc Natl Acad Sci 87:1648–1652

Cowles TJ, Desiderio RA (1993) Resolution of biological microstructure through *in situ* fluorescence emission spectra. Oceanography 6:105–111

Cowles TJ, Desiderio RA, Carr ME (1998) Small-scale planktonic structure: persistence and trophic consequences. Oceanography 11:4–9

Davis CS, Gallager SM, Solow AR (1992) Microaggregations of oceanic plankton observed by towed video microscopy. Science 257:230–232

Denman KL, Powell TM (1984) Effects of physical processes on planktonic ecosystems in the coastal ocean. Oceanogr Mar Biol Annu Rev 22:125–168

Donaghay PL, Rines HM, Sieburth JM (1992) Simultaneous

sampling of fine scale biological, chemical, and physical structure in stratified waters. Ergeb Limnol 36:97–108
Eckart C (1948) An analysis of the stirring and mixing processes in incompressible fluids. J Mar Res 7:265–275
Eppley RW, Holmes RW, Strickland JDH (1967) Sinking rates of marine phytoplankton measured with a fluorometer. J Exp Mar Biol Ecol 1:191–208
Fasham MJR (1978) The application of some stochastic processes to the study of plankton patchiness. In: Steele JH (ed) Spatial pattern in plankton communities. Plenum Press, New York, p 131–156
Fraga S, Gallager SM, Anderson DM (1988) Chain-forming dinoflagellates: an adaptation for red tide formation. In: Okaichi T, Anderson DM, Nemoto T (eds) Red tides: biology, environmental science and toxicology. Elsevier, Amsterdam, p 281–284
Franks PJS (1995) Thin layers of phytoplankton: a model of formation by near-inertial wave shear. Deep-Sea Res 42:75–91
Gallager SM, Davis CS, Epstein AW, Solow A, Beardsley RC (1996a) High-resolution observations of plankton spatial distributions correlated with hydrography in the Great South Channel, Georges Bank. Deep-Sea Res Part II Top Stud Oceanogr:1627–1663
Gallager SM, Manuel JL, Manning DA, O'Dor R (1996b) Ontogenetic changes in the vertical distribution of scallop larvae *Placopecten magellanicus* in 9 m deep mesocosms as a function of light, food, and temperature. Mar Biol 124: 679–692
Gargett AE (1989) Ocean turbulence. Annu Rev Fluid Mech 21:419–451
Gargett AE, Osborn TR, Nasmyth PW (1984) Local isotropy and the decay of turbulence in a stratified fluid. J Fluid Mech 144:231–280
Hardy AC, Bainbridge R (1954) Experimental observations on the vertical migrations of plankton animals. J Mar Biol Assoc UK 33:409–448
Hardy AC, Gunther ER (1935) The plankton of the south Georgia whaling grounds and adjacent waters. Discov Rep 11:1–456
Hill PS, Nowell ARM, Jumars PA (1992) Encounter rate by turbulent shear of particles similar in diameter to the Kolmogorov scale. J Mar Res 50:643–668
Houghton RW, Schlitz R, Beardsley RC, Butman B, Chamberlain JL (1982) The middle Atlantic Bight cold pool: evolution of the temperature structure during 1979. J Phys Oceanogr 12:1019–1029
Kullenberg G (1978) Vertical processes and the vertical-horizontal coupling. In: Steele JH (ed) Spatial pattern in plankton communities. Plenum Press, New York, p 43–72
Kundu PK (1990) Fluid mechanics. Academic Press, San Diego
Kundu PK, Beardsley RC (1991) Evidence of a critical Richardson number in moored measurements during the upwelling season off northern California. J Geophys Res 96:4855–4868
Lande R, Wood M (1987) Suspension time of particles in the upper ocean. Deep-Sea Res 34:61–72
Levandowsky M, Kaneta PJ (1987) Behavior in dinoflagellates. In: Taylor FJR (ed) The biology of dinoflagellates. Oxford Press, Oxford, p 360–398
MacIntyre S, Alldredge AL, Gotschalk CC (1995) Accumulation of marine snow at density discontinuities in the water column. Limnol Oceanogr 40:449–468
Mackas DL, Denman KL, Abbott RA (1985) Plankton patchiness: biology in the physical vernacular. Bull Mar Sci 37: 652–674
Moum JM (1996) Energy-containing scales of turbulence in the ocean. J Geophys Res 101:14095–14109
Ochoa J (1987) Two limiting types of oceanic finestructure. J Phys Oceanogr 17:1539–1545
Osborn T (1998) Finestructure, microstructure, and thin layers. Oceanography 11:36–43
Osborn T, Farmer DM, Vagle S, Thorpe SA, Cure M (1992) Measurements of bubble plumes and turbulence from a submarine. Atmos Ocean 30:419–440
Owen RW (1989) Microscale and finescale variations of small plankton in coastal and pelagic environments. J Mar Res 47:197–240
Pineda J (1991) Predictable upwelling and the shoreward transport of planktonic larvae by internal tidal bores. Science 253:548–551
Pollard RT (1977) Observations and theories of Langmùir circulations and their role in near surface mixing. In: Angel M (ed) A voyage of discovery. Pergamon Press, Oxford
Rothschild BJ, Osborn TR (1988) Small-scale turbulence and plankton contact rates. J Plankton Res 10:465–474
Saiz E (1994) Observations on the free-swimming behaviour of the copepod *Acartia tonsa*: effects of food concentration and turbulent water. Limnol Oceanogr 39:1566–1578
Seim HE, Gregg MC (1994) Detailed observation of a naturally occurring shear instability. J Geophys Res 99:10049–10073
Shanks AL, Largier L, Brink L, Brubaker J, Hooff R (2000) Demonstration of the onshore transport of larval invertebrates by the shoreward movement of an upwelling front. Limnol Oceanogr 45:230–236
Sieracki ME, Gifford DJ, Gallager SM, Davis CS (1998) Ecology of a *Chaetoceros socialis* Lauder patch on Georges Bank: distribution, microbial associations, and grazing losses. Oceanography 11:30–35
Squires K, Yamazaki H (1995) Preferential concentration of marine particles in isotropic turbulence. Deep-Sea Res Part II Top Stud Oceanogr 42:1989–2004
Strickler JR (1998) Observing free-swimming copepods mating. Phil Trans R Soc Lond B Biol Sci 353:671–680
Tennekes H, Lumley JL (1972) A first course in turbulence. MIT Press, Cambridge
Tiselius P, Jonsson PR, Verity PG (1993) A model evaluation of the impact of food patchiness on foraging strategy and predation risk in zooplankton. Bull Mar Sci 53:247–264
Tsuda A, Miller CB (1998) Mate-finding behaviour in *Calanus marshallae* Frost. Phil Trans R Soc Lond B Biol Sci 353: 713–720
Van Duren LA, Stamhuis EJ, Videler JJ (1998) Reading the copepod personal ads: increasing encounter probability with hydromechanical signals. Phil Trans R Soc Lond B Biol Sci 353:691–700
Weissburg MJ, Doall MH, Yen J (1998) Following the invisible trail: kinematic analysis of mate-tracking in the copepod *Temora longicornis*. Phil Trans R Soc Lond B Biol Sci 353:701–712
Yamazaki H, Kamykowski D (1991) The vertical trajectories of motile phytoplankton in a wind-mixed water column. Deep-Sea Res 38:219–241
Yamazaki H, Osborn T (1993) Direct estimation of heat flux in a seasonal thermocline. J Phys Oceanogr 23:503–516
Yamazaki H, Squires KD (1996) Comparison of oceanic turbulence and copepod swimming. Mar Ecol Prog Ser 144:299–301
Yamazaki H, Mackas D, Denman K (2002) Coupling small scale physical processes with biology: towards a Lagrangian approach. In: Robinson AR, McCarthy JJ, Rothschild BJ (eds) The sea: biological-physical interaction in the ocean, Vol 12. John Wiley & Sons, New York, p 51–112
Yen J, Weissburg MJ, Doall MH (1998) The fluid physics of signal perception by mate-tracking copepods. Phil Trans R Soc Lond B Biol Sci 353:787–804

Editorial responsibility: Otto Kinne (Editor), Oldendorf/Luhe, Germany

Submitted: October 20, 2000; Accepted: August 31, 2003
Proofs received from author(s): February 9, 2004